A Comprehensive Conformational Analysis of Bullacin B, a Potent Inhibitor of Complex I. Molecular Dynamics Simulations and *Ab Initio* Calculations

José A. Bombasaro,[†] Marcelo F. Masman,[†,‡] Luis N. Santágata,[†] Mónica L. Freile,[§] Ana M. Rodríguez,[†] and Ricardo D. Enriz*[,†,‡]

Facultad de Química, Bioquímica y Farmacia, Universidad Nacional de San Luis (UNSL) and IMIBIO-SL, Chacabuco 917, 5700 San Luis, Argentina, and Facultad de Ciencias Naturales, Universidad Nacional de la Patagonia San Juan Bosco (UNPSJB), Km 4. Comodoro Rivadavia, 9000 Chubut, Argentina

Received: December 11, 2007; Revised Manuscript Received: June 5, 2008

Using a conformational systematic search combined with semiempirical and *ab initio* (RHF/3-21G and RHF/6-31G(d)) calculations, the conformational space of bullacin B was examined for the first time. In addition, molecular dynamics simulations were carried out to better evaluate the conformational behavior of this acetogenin. Our results indicate that bullacin B possesses a significant molecular flexibility. Although many different conformations were identified, at *ab initio* level, the L forms were energetically mostly preferred. Our results support the use of molecular dynamics simulations for this compound suggesting that a combined decane/water system is a good solvent system to simulate the biological environment of this molecule acting as inhibitor of complex I.

1. Introduction

1.1. Biological Background. Acetogenins (ACGs) have very potent and diverse biological effects including cytotoxic, antitumor, antimalarial, pesticidal, and antifeedant activities.[1–3] The inhibitory effects of ACG on mitochondrial NAD-ubiquinone oxidoreductase (complex I) are of particular note, as the diverse biological activities are thought to be attributable to this effect.[1,4–7] In fact, some of these compounds, such as bullacin B (Figure 1) and rolliniastatin-1, are the most potent inhibitors of this enzyme identified to date.[7–9]

It is very difficult to visualize structural similarities between the ACGs and ordinary complex I inhibitors such as piericidin A and rotenone, although the ACGs act as the terminal electron transfer step of complex I, similarly to the ordinary complex I inhibitors.[6,7,9] The ACGs are fairly large molecules compared with the ordinary complex I inhibitors including some potent agrochemicals such as Fenpyroximate and SAN548A.[8]

The chemical structure of most natural ACGs is characterized by four segments, namely, an α,β-unsaturated γ-lactone ring (LR), one to three tetrahydrofuran (THF) ring(s) with flanking OH group(s), a long alkyl tail, and an alkyl spacer linking the γ-lactone and the THF moieties (Figure 1). Miyoshi and colleagues,[5,10] as well as other groups,[11,12] have reported studies of the structure−activity relationship (SAR) using systematically selected natural and synthetic ACGs. On the basis of those results, Abe et al.[13] have reported that an α,β-unsaturated γ-lactone ring, a structural feature common to a large number of natural ACG, is not crucial for the activity and may be replaced with other structures.[10–14] With respect to the hydroxylated THF ring moiety, neither the number of THF rings nor the stereochemistry around this portion is an essential factor.[5,10–19] The presence of either of the two OH groups adjacent to the THF ring(s) sustains sufficiently the potent activity.[20] A long tail is preferable but not essential, since even a methyl derivative elicits strong inhibition at the nanomolar level.[21] An interesting further development is the discovery that neither of the two independently synthesized components of the inhibitor, the hydroxylated bis-THF ring with two alkyl chains and the LR with an alkyl chain, has an inhibitory effect by itself and there is no synergistic enhancement of the inhibitory activity between the two components.[22,23] Thus, ACG appears to act as a potent inhibitor only when the LR and the THF ring moieties are directly linked by an alkyl spacer and the optimal length of the spacer would be of about 13 carbon atoms. These results strongly suggest that both ring moieties act in a cooperative manner on the enzyme with the support of some specific conformation of the spacer.

Based on the results of ^{1}H NMR spectroscopic and differential scanning calorimetry studies of acetogenins in liposomal membranes, McLaughlin and colleagues[24,25] have proposed the model of an active conformation of these inhibitors in the membrane environment. A THF ring(s) with flanking hydroxy groups resides near the glycerol backbone of phosphatidylcholine irrespective of the number of THF rings and acts as a hydrophilic anchor at the membrane surface. On the other hand, the LR interacts directly with the target site of complex I, probably the ubiquinone reduction site,[9] by lateral diffusion in the mitochondrial membrane interior, as illustrated in Figure 2. Molecular dynamic calculations of diacetyl-guanacone in a full hydrated l-palmitoyl-2-oleoyl-*syn*-glycero-3-phosphatidylcholine (POPC) bilayer have been recently reported by our research group.[26] Molecular dynamics (MD) simulation reveals the presence of hydrogen bonds, which are critical to adopt a particular conformation, and indicates the important role of THF rings and the flanking acetyl groups for the geometry of this molecule.

1.2. The Conformational Problem. Exploration of the conformational space, if exhaustive, may become a formidable task, since variations of dihedral angles induce a tremendously large number of internal degrees of freedom, even for a medium-size molecule such as bullacin B. This compound is a multiple

* To whom correspondence should be addressed. Telephone: +54-2652-423789. Fax: +54-2652-431301. E-mail: denriz@unsl.edu.ar.
† Universidad Nacional de San Luis.
‡ IMIBIO-CONICET, UNSL.
§ Universidad Nacional de la Patagonia San Juan Bosco.

10.1021/jp801962x CCC: $40.75
Published on Web 07/24/2008

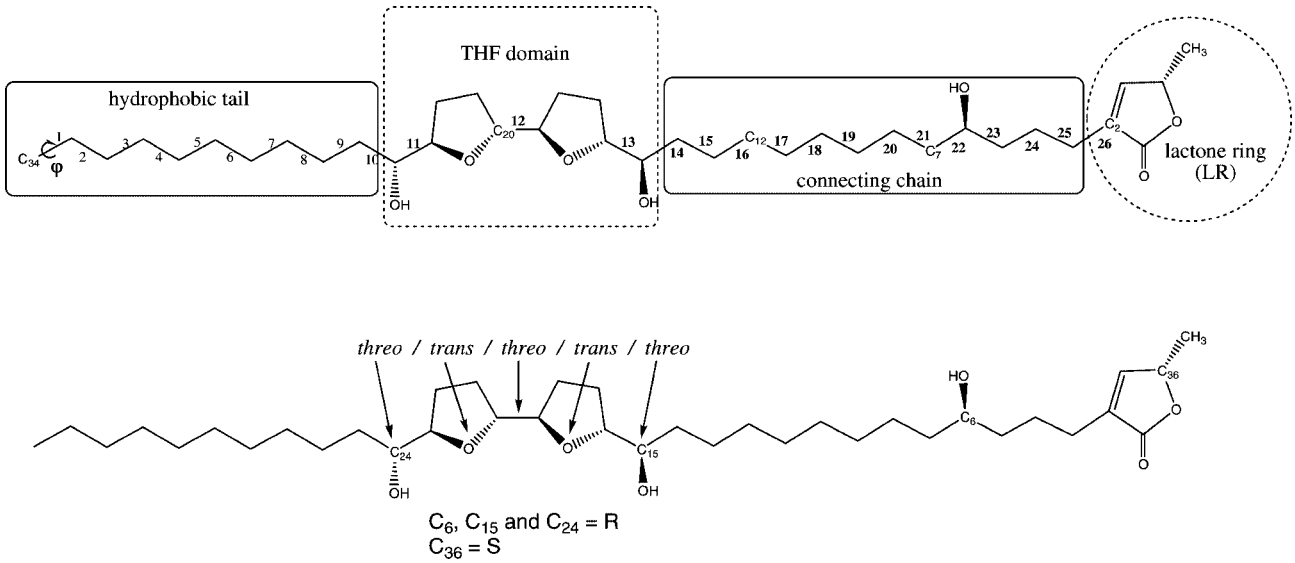

Figure 1. Structural feature of bullacin B showing the 26 torsional angles (in bold). The different segments of bullacin B are also shown in this figure (top). The relative stereochemistry across the rings, obtained from ref 30, is illustrated at the bottom.

rotor, and therefore, the overall expression of the conformational potential energy hypersurface (PEHS) is the function of 26 circular motions involving $\varphi_1-\varphi_{26}$ torsional angles (Figure 1). Multidimensional conformational analysis (MDCA)[27,28] predicts the existence of 1.69×10^{12} legitimate minima for a multiple rotor possessing 26 rotations with their corresponding multiplicities. The problem is even more complex if the different isomers are to be analyzed considering the stereochemistry around the THF and the LR. Thus, a complete and systematic conformational analysis of bullacin B using *ab initio* calculations appears to be, at least in principle, an extremely difficult task. Fortunately, significant simplifications can be performed in order to evaluate the overall conformational behavior of this compound. A previously reported SAR study[29] indicates that the stereochemistry around the THF and LR moieties is not an essential factor for the activity. Therefore, only one configurational isomer of bullacin B is analyzed in our study which was selected from experimental results.[30] In addition, Motoyama et al.[21] demonstrated that the presence of a long alkyl tail is preferable but not essential; therefore, we can keep this part of the molecule in an extended form at least for the *ab initio* calculations. Thus, the 26 torsion angles can be reduced to 15 torsional modes (torsion angles 13-26 in Figure 1). MDCA predicts 9 565 938 potentially legitimate minima for a multiple rotor possessing 15 rotations. Even with this reduction, it is clear that the conformational problem of bullacin B is still very complex.

It has been demonstrated that the spacer moiety (connecting chain) is very important for the potent activity. This finding, however, does not necessarily indicate that the distance itself, between the THF ring(s) and the LR, is important for the inhibitory effect, since the activities of the compounds which have the same or similar number of carbon atoms in the spacer often differ markedly.[13] Therefore, some sort of specific conformation of the spacer might regulate the two ring moieties to be located into an optimal spatial position, which is essential to elicit the most potent inhibition. Thus, the understanding of the conformational intricacies of the alkyl spacer linking the LR and THF rings might be helpful to elucidate the optimal conformation of the ACG as well as the function of this spacer. Also, it would be very important to determine the "biologically relevant" conformation of the ACG.

A great number of studies have been performed in order to shed some light on the structural features and bioactivities of ACG and their congeners.[5–12] However, unlike these aspects, the conformational intricacies of these compounds have received relatively little attention. To the best of our knowledge, only one paper has been reported by Miyoshi et al.[29] using semiempirical calculations to evaluate the conformational behavior of ACG. However, in that paper, the authors concentrated their efforts in the stereochemical aspects of THF rings but not in the overall conformational problem. The aim of the present study is to examine the PEHS of bullacin B using two different approaches. In a first step, a systematic conformational search using semiempirical computations combined with *ab initio* (RHF/3-21G and RHF/6-31G(d)) calculations is performed. Next, the conformational study is complemented using MD simulations. In the calculation method section, the steps followed using several approaches are described. The ability of each method to obtain the different conformations is tested and compared.

2. Methods of Calculation

As was previously mentioned, two different approaches were used in the conformational study. First, a thorough exploration was performed using a systematic search procedure using the geometrical algorithm GASCOS[31] combined with semiempirical and *ab initio* calculations. In a second step, MD simulations using two different solvents were carried out.

2.1. Systematic Conformational Search Combined with Semiempirical and *Ab Initio* Calculations. Systematic search methods (or so-called grid search methods to remember the stepwise variations of independent geometrical parameters) look appealing, since they lead to an exhaustive generation of possible conformers. However, for systems with numerous degrees of freedom (such as bullacin B), a systematic study would rapidly become a formidable task in order to ensure that interesting conformations have been overlooked. Considering the significant number of torsional angles involved in our study and with the aim to maintain the number of conformations in a "manageable" quantity, 120° dihedral angle resolution seems convenient in this case. We have used previously this resolution successfully in small size compounds.[32,33]

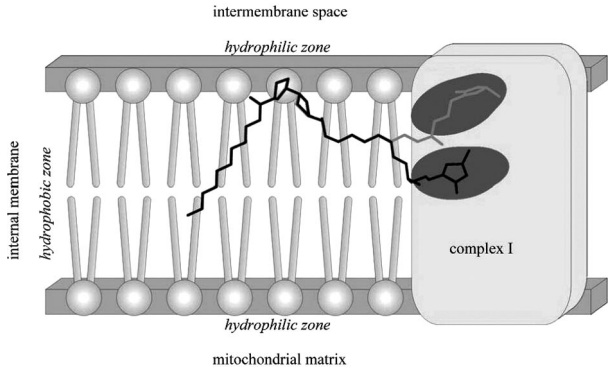

Figure 2. Model of the potentially active conformation of bullacin B interacting with complex I in the mitochondrial membrane proposed by McLaughlin et al.[24]

SCHEME 1: Different Steps and General Results Obtained with the Systematic Conformational Search

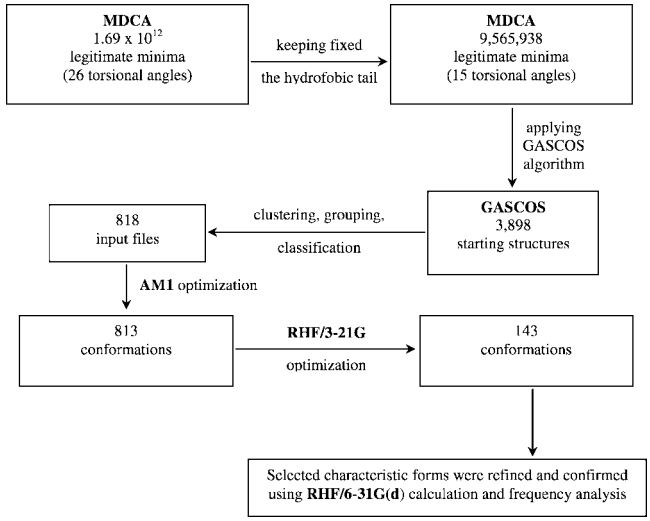

The search for minimum-energy conformations was carried out in four discrete steps. In the first step, a systematic conformational search to obtain the geometrically available forms was carried out using the GASCOS algorithm. In the second step, these geometries were subjected to classification, grouping and clustering using the GASCOS program. In the third step, the starting points suggested by GASCOS were optimized using AM1[34] calculations. In the fourth step, minimum energy conformations obtained from AM1 were refined using the RHF/3-21G level. Finally, characteristic conformations were selected (see section 3.1) to optimize using RHF/6-31G(d) calculations and frequency analysis.

In Scheme 1, the steps and general results obtained with the systematic conformational search are summarized. MDCA predicts 1.69×10^{12} potential minima considering 26 torsional angles. However, keeping the hydrophobic tail fixed, MDCA predicts 9 565 938 potential minima for bullacin B, which is still an amazing number of conformations to calculate. Keeping the hydrophobic tail fixed, the GASCOS algorithm predicts 3898 possible geometries for bullacin B (Table 1). Next, these geometries were subjected to classification, grouping, and clustering. The conformations generated by the grid-scan procedure were clustered to obtain a smaller set of conformers that would reliably represent the conformational space.

To categorize the obtained structures we introduced, intuitively rather than by a precise definition, five general forms (families): V, LC (L, closed), L, LO (L, open), and the extended

TABLE 1: 3898 Geometries Predicted by GASCOS Grouped in 5 Families and 25 Subfamilies

	subfamily						
		angle ε					
family	angle δ	v	lc	l	lo	i	total structures
V	v	0	0	1	7	3	465
	lc	0	12	27	30	50	465
	l	2	12	33	26	68	465
	lo	2	2	18	40	32	465
	i	4	20	40	20	16	465
LC	v	0	0	0	4	6	726
	lc	0	7	22	16	54	726
	l	2	4	24	32	66	726
	lo	2	2	36	44	78	726
	i	1	14	64	70	178	726
L	v	0	0	2	2	4	1113
	lc	0	6	12	20	48	1113
	l	0	14	56	58	90	1113
	lo	4	2	58	104	84	1113
	i	3	12	142	146	246	1113
LO	v	0	0	0	6	5	589
	lc	0	4	8	18	48	589
	l	0	2	40	22	68	589
	lo	0	2	20	56	78	589
	i	2	14	68	56	72	589
I	v	0	0	2	4	8	1005
	lc	0	12	36	28	66	1005
	l	2	16	44	54	104	1005
	lo	4	4	48	74	76	1005
	i	5	24	100	86	208	1005

I family, considering their obvious similarity with the respective letters (see Figure 3). These families were classified according to the spatial orientation adopted by the molecule. We defined two virtual axes $C_{34}-C_{20}$ and $C_{20}-C_2$, which determine the γ virtual angle. The values of this angle defined the five different families (Scheme 2). However, this general classification is not enough to obtain comprehensive information about the different spatial orderings adopted by the connecting chain. Thus, in order to get meaningful information about the orientations of this

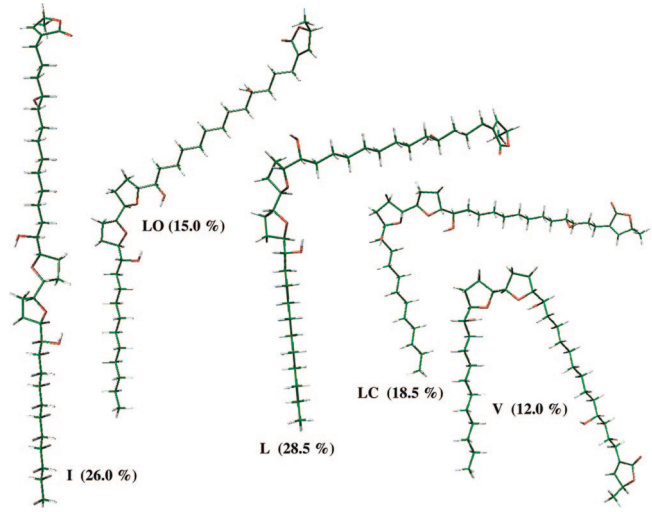

Figure 3. Spatial view showing the characteristic forms of each family. In these structures, the hydrophobic tail and the connecting chain were kept extended for clarity. The percentage of populations obtained from GASCOS algorithm is shown in parentheses.

SCHEME 2: Scheme Defining the Families and Subfamilies as a Function of the Different Values of Virtual Angles γ, δ, and ε

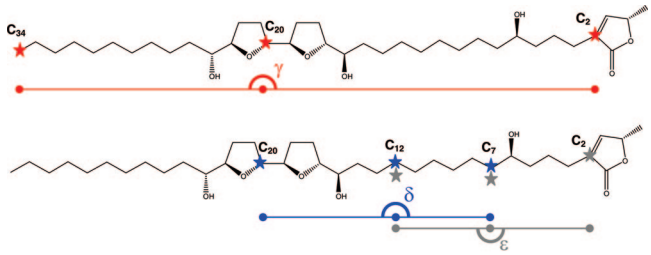

	family		sub-family
V	$\gamma \sim 0° - 75°$	V	$\delta / \varepsilon \sim 0° - 75°$
LC	$\gamma \sim 75° - 95°$	LC	$\delta / \varepsilon \sim 75° - 95°$
L	$\gamma \sim 95° - 115°$	L	$\delta / \varepsilon \sim 95° - 115°$
LO	$\gamma \sim 115° - 130°$	LO	$\delta / \varepsilon \sim 115° - 130°$
I	$\gamma \sim 130° - 180°$	I	$\delta / \varepsilon \sim 130° - 180°$

moiety, two new virtual angles were defined using two new virtual axes. Angle δ was defined using virtual axes $C_{20}-C_{12}$ and $C_{12}-C_7$, whereas angle ε was defined from virtual axes $C_{12}-C_7$ and C_7-C_2. The different values adopted by angles γ, δ, and ε defined 125 different subfamilies (Table 1). The fully folded form displayed the three virtual angles (γ, δ, and ε) in V (subfamily $V_{V,V}$), whereas the fully extended form showed these angles in I (subfamily $I_{I,I}$). Thus, the different forms were included in their respective subfamilies according to their general spatial ordering which resembled one of the letters previously defined. It must be pointed out that the hydrophobic tail was kept in an extended form in this systematic conformational search. Among the conformations obtained, we observed conformations possessing a fully extended connecting chain (they had all the torsion angles of the connecting chain near 180°) and conformations possessing different combinations of folded ($\cong \pm 60°$) and extended ($\cong 180°$) torsional angles in this moiety.

In addition, to better evaluate the molecular flexibility of bullacin B, rotational energy profiles around the most representative torsional angles have been determined from RHF/6-31G(d) and IPCM calculations (IPCM//RHF/6-31G(d)) using reduced model systems. The energy has been calculated at 15° intervals of the analyzed dihedral angles. The effect of the solvent (water) was calculated by the isodensity polarizable continuum model (IPCM) method.[35] IPCM is more advanced than the polarizable continuum model (PCM) method[36] because in IPCM the cavity of a solute is defined by the electron isodensity surface while in PCM it is defined by the van der Waals surface. The efficiency of this method has been widely recognized in chemical behaviors in solution for small polar molecules.[37–42] It should be emphasized, however, that the evaluation of the solvent effect implies a comparison with the gas-phase results. Thus, both sets of results, with and without the solvent, are required.

Geometry optimizations of bullacin B were carried out using both AM1 and *ab initio* RHF/3-21G methods. These calculations were performed utilizing the Gaussian03 program.[43] In order to assess the performance of these approaches, characteristic conformations were computed at a higher theoretical level. Thus, the RHF/3-21G outputs were used as inputs for the RHF/6-31G(d) calculations. Low-energy conformations were confirmed from a vibrational frequency analysis using RHF/6-31G(d) calculations.

The electronic study of bullacin B was carried out using molecular electrostatic potentials (MEPs). MEPs have been shown to provide reliable information, both on the interaction sites of molecules with point charges and on the comparative reactivities of these sites.[44–46] These MEPs were calculated by using RB3LYP/6-31G(d) wave functions. Single point calculations were performed on the RHF/6-31G(d) geometries in order to obtain the MEPs. MEP graphical presentations were created using the Molekel program.[47]

2.2. Molecular Dynamics Calculations. MD can also be used to derive low-energy conformers. Basically, whereas X-ray and other theoretical methods give a static time averaged picture of atomic locations, MD simulates their instantaneous motions.[48–50] Atom coordinates change with time, depending upon the kinetic energy terms and forces exerted by surrounding atoms. Over short periods of time, motions may be erratic, but over longer periods coherent collective motions may be distinguished, giving some insight about preferred local fluctuations of selected groups. From these trajectories, low-energy structures may be periodically sampled, giving some insight about conformational changes.[48]

MD simulations from different starting points or using simulated annealing have not been performed. Thus, we do not expect that the entire dynamic conformational behavior of bullacin B be explained by such reduced treatment. The aim of these calculations is less ambitious. We intend to obtain a reasonable indication of the direction and magnitude of changes in the conformational preferences of the molecule when it enters in different solvents (water and decane/water).

MD simulations and the trajectory analysis were performed using the GROMACS 3.2.1 programs package.[51,52] The GROMACS[53–57] united-atoms force field (FF) and the SPC water model[58,59] were used. The time step for the simulations was 0.002 ps. For long-ranged interactions, the article-mesh Ewald (PME)[60–62] method was used with a 1 nm cutoff and a Fourier spacing of 0.12 nm. The MD protocol consisted of several preparatory steps: energy minimization using the conjugate gradient model,[63,64] density stabilization (NVT conditions), and finally production of the MD simulation trajectory. All production simulations were performed under NPT conditions at 300.0 K and 1.0 bar, using Berendsen's coupling algorithm[65] for keeping temperature ($\tau_T = 0.1$ ps) and pressure ($\tau_P = 0.5$ ps) constant. The compressibility was 4.8×10^{-5} bar^{-1}. All coordinates were saved every 5.0 ps. The SETTLE[58] algorithm was used to keep water molecules rigid during MD simulations. The LINCS[66] algorithm was used to constrain all length bonds in the preparatory steps. However, no restrains were used in production-MD simulations. A length of 50.0 ns was taken in to account for all production-MD simulations.

Two different molecular systems were studied. On one hand, the conformational behavior of bullacin B in water was examined. On the other hand, a simulation with bullacin B embedded in the water/decane interface was performed. In the first system, bullacin B was embedded in a box containing 4340 water molecules with at least 1 nm between the solute and the edge of the box resulting in a box of 5.13 nm of side lengths. The second system consisted of a biphasic environment in which the conformational behavior of bullacin B was examined. This biphasic system consisted of 188 decane molecules and 1468 water molecules; the size of the simulation box was 4.36 nm in the x and y directions, and 5.42 nm in the z direction. This system was built up in such a way that all decane molecules were forming a layer located near the middle of the box (ca. 2.71 nm in the z direction) whereas water molecules were above and below the decane layer (Scheme 3). The thickness of the decane layer was ~2.96 nm. Just then, the solvent (decane and water) molecules were correctly localized into the box. An

SCHEME 3: Initial Configuration[a]

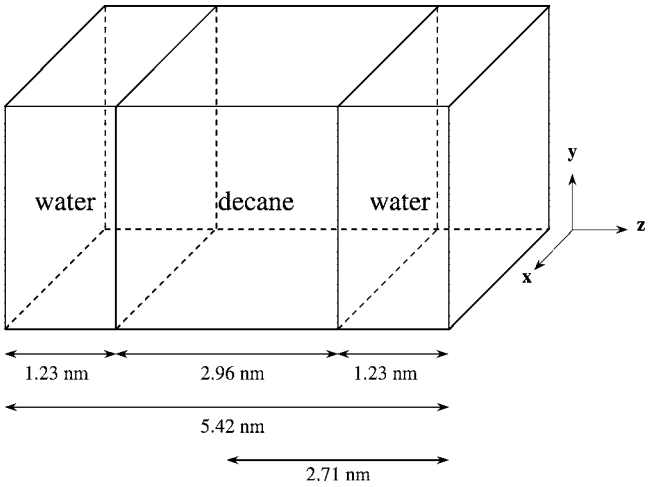

[a] Decane is in the middle, and water is on both the left and right side of the box. The *z* axis is chosen to be perpendicular to the interface.

TABLE 2: Percentage of Populations (%) Obtained for the Five Families of Bullacin B Using GASCOS, AM1, RHF/3-21G, and MD Calculations

families	GASCOS[a]	GASCOS[b]	AM1[c]	AM1[d]	RHF/3-21G	MD[e]
V	12.0	17.5	11.5	14.0	18.0	82.0
LC	18.5	18.5	17.0	10.5	12.0	9.0
L	28.5	20.5	27.0	34.0	31.0	4.5
LO	15.0	18.5	15.0	9.5	14.0	2.5
I	26.0	25.0	29.5	32.0	25.0	2.0

[a] From 3898 structures. [b] From 818 structures. [c] From 813 structures. [d] Considering an energy window of 2.5 kcal·mol^{-1}. [e] From a simulation in decane/water system.

energy minimization and an NVT-MD simulation of 10 ns long were performed in order to equilibrate the interfaces formed between solvent molecules. After the solvent stabilization was reached, a molecule of bullacin B was embedded into the decane/water interface. An extra step of prestabilization of 1 ns long was performed before the production-MD simulation was started.

3. Results and Discussion

3.1. Exploration of the Conformational Space of Bullacin B (Systematic Conformational Search). The 3898 geometries obtained from the GASCOS algorithm were distributed in a fairly homogeneous way among the five different families (see the number of structures in Table 1 and percentage of populations in Table 2), with the L and I forms being the most populated families with 28.5 and 26.0%, respectively. Table 1 shows the absence of type $X_{V,V}$ subfamilies (with X being any of the five families). This result appears to be reasonable considering that these forms adopted a very intricate spatial ordering. Once all the geometries obtained from GASCOS were clusterized, to further reduce the input files, a representative number of structures for each subfamily was chosen. Ten geometries were randomly selected for each subfamily when the number was larger than 10, whereas in the cases in which the number of geometries was lower than 10, all of them were used as input files. Thus, 818 geometries were obtained, which were used as starting structures for AM1 optimizations. It should be noted that the percentage of the population obtained for these 818 geometries was closely related to those previously attained for the 3898 initial geometries (comparing first and second columns in Table 2).

TABLE 3: 813 Conformations Obtained from AM1 Optimizations Grouped in 5 Families and 25 Subfamilies

	subfamily						
	angle ε						
family	angle δ	v	lc	l	lo	i	total structures
V	v	0	0	5	4	1	86
	lc	0	10	7	0	1	86
	l	4	9	3	5	8	86
	lo	2	2	3	6	4	86
	i	0	1	3	4	4	86
LC	v	0	0	1	0	5	138
	lc	0	2	7	2	7	138
	l	1	0	3	5	12	138
	lo	1	0	7	10	11	138
	i	0	5	11	13	35	138
L	v	0	0	2	1	3	219
	lc	0	11	4	2	8	219
	l	1	6	5	12	19	219
	lo	0	3	9	16	17	219
	i	0	14	17	25	53	219
LO	v	0	1	4	0	0	127
	lc	0	1	0	0	1	127
	l	1	0	3	6	9	127
	lo	1	2	4	11	16	127
	i	1	4	11	16	35	127
I	v	0	0	1	5	0	243
	lc	1	8	5	2	1	243
	l	5	8	2	12	5	243
	lo	3	2	10	16	3	243
	i	3	9	13	20	3	243

The results obtained from AM1 optimizations are summarized in Table 3 and Table S1 of the Supporting Information. Eight-hundred and thirteen conformations were obtained from AM1 optimizations. AM1 calculations suggested a relatively homogeneous distribution among the five families, with the I and L families being the most populated ones (see percentage of populations in Table 2). These two families were also the energetically preferred conformations, with an $L_{I,I}$ conformer being the global minimum. It is interesting to note that AM1 calculations predicted very low-energy gaps between the low-energy conformations. Thus, considering an energy window of 2.5 kcal·mol^{-1}, the five families were represented (see Table S1 in the Supporting Information). Table 3 and Table S1 of the Supporting Information show that AM1 optimizations preferred those conformations possessing the connecting chain in fully extended or partially extended forms. This result might be appreciated from the significant populations obtained in the $X_{I,I}$ boxes (fully extended connecting chain) as well as in the $X_{I,LO}$ and $X_{I,L}$ boxes (partially extended connecting chain, in Table 3). These forms were the energetically preferred conformations for the AM1 optimizations.

In the next step, RHF/3-21G optimizations were performed using the preferred conformations obtained from AM1 calculations as input files. The 77 preferred forms obtained from AM1 were optimized, considering an energy window of 2.5 kcal·mol^{-1} (Table S1 in the Supporting Information). However, there are many subfamilies which were not represented within this window. Therefore, for the RHF/3-21G calculations, several of these subfamilies were included in order to evaluate a more representative sample of conformers. Thus, 186 RHF/3-21G calculations were performed, obtaining 143 different conformers (Table S2 in the Supporting Information). There were 12 input

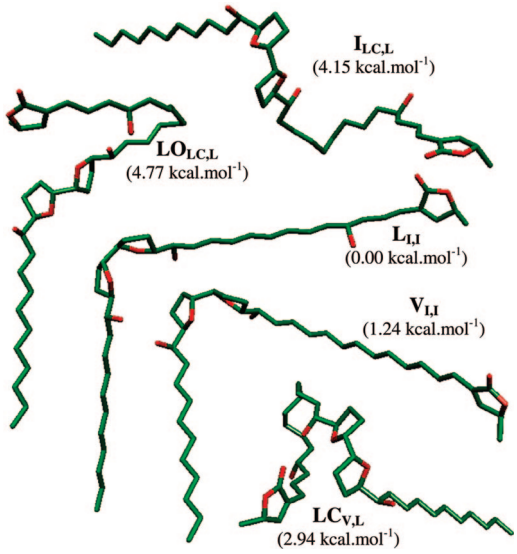

Figure 4. Spatial view of the preferred conformations of each family obtained from RHF/6-31G(d) optimizations. ΔE_{rel} values are shown in parentheses. All hydrogens are omitted for clarity.

files that did not converge, and the rest migrated to a previously obtained conformation. Comparing the percentage of populations obtained from AM1 (considering an energy window of 2.5 kcal·mol^{-1}) and RHF/3-21G calculations, it appears that both results are comparable (Table 2). However, analyzing the semiempirical and *ab initio* results in more detail, important differences might be appreciated. The energy gaps among the different conformers obtained from *ab initio* results were markedly higher with respect to those attained using AM1 calculations (Tables S1 and S2 in the Supporting Information). RHF/3-21G calculations suggested that an $LO_{LC,LC}$ form was the global minimum and in general the LO, L, and LC families were the preferred ones. The extended $I_{I,I}$ form of the lowest energy possessed 7.67 kcal·mol^{-1} above the global minimum, indicating that these fully extended conformations were not energetically preferred for the *ab initio* calculations. This shows a striking difference between the semiempirical and *ab initio* calculations. During the *ab initio* calculations, many "migrations" were observed. By "migration", we mean that a starting AM1 geometry is changed to another form as a consequence of the *ab initio* optimization. Different types of "migrations" were observed, but in general, at the *ab initio* level, there was a tendency to somewhat fold the conformers.

Finally, we chose the lowest-energy conformation obtained for each family (V, LC, L, LO, and I) from RHF/3-21G optimizations, and we optimized them using RHF/6-31G(d) calculations. In addition, a frequency analysis was carried out for these conformations to confirm that they were true minima in the potential energy hypersurface. Figure 4 gives a spatial view of the conformations of bullacin B obtained from RHF/6-31G(d) calculations for each family. RHF/6-31G(d) calculations indicated that $L_{I,I}$ was the energetically preferred form, which was in agreement with the semiempirical results.

The conformational analysis of bullacin B requires at this point the evaluation of the molecular flexibility, that is, the energy determinations of the transitional barrier between the different conformers. This is of crucial importance because if these barriers are low during molecular recognition, bullacin B might be converted with a low energy cost to a preferred conformation in the binding site within complex I. Three model systems (Scheme 4) were used to mimic characteristic parts of

SCHEME 4: Scheme of Reduced Model Systems Showing the Torsional Angles θ_1−θ_5

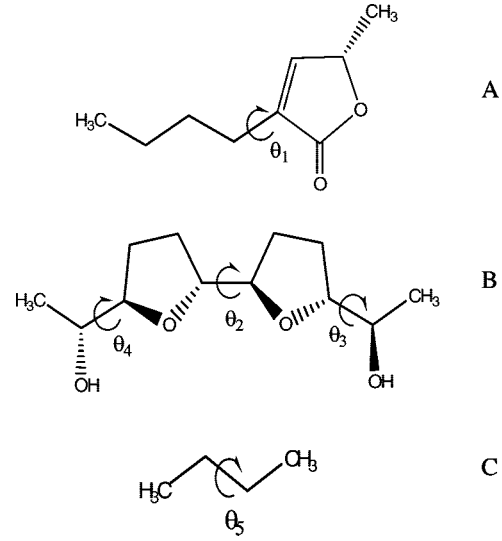

bullacin B and other ACGs and to perform quantum mechanical (QM) molecular orbital (MO) calculations. The use of model systems to calculate the potential energy surfaces (PESs) and the potential energy curves (PECs) is necessary, since bullacin B is too large for accurate QM/MO calculations. By using a model, dealing with complexities due to the rest of the molecule is avoided. Thus, a better understanding of the inherent conformational properties of the different moieties of bullacin B reflected in the PESs and PECs may be gained. When choosing a model system, the ability to reproduce conformational properties of the entire molecule was considered. In this study, we mainly considered the following five torsion angles: θ_1 (LR torsion, Scheme 4A), θ_2 (THF torsion), θ_3 and θ_4 (the first torsional angle of the connecting chain and the hydrophobic tail, respectively, Scheme 4B), and θ_5 (torsion between methylene groups, Scheme 4C).

It is clear that the dihedral angles θ_2, θ_3, and θ_4 interconnecting the two THF rings seem to have a central role in determining the overall fold of bullacin B. Thus, we evaluated the PES scanning θ_2 versus θ_3 (Figure 5). Both θ_2 and θ_3 angles were varied in 15° increments and were constrained during the subsequent energy minimization with respect to all other internal coordinates. Nine clearly defined potential wells, corresponding to regions close to the expected nine (θ_2 and θ_3) rotamers, can be seen in this figure. It should be noted that MDCA predicted 27 different conformations for the reduced system considering three dihedral angles (θ_2, θ_3, and θ_4, Scheme 4B). We calculated these 27 conformations, and all of them were obtained from RHF/6-31G(d) calculations (Table S3 in the Supporting Information). Interestingly, all these conformations had been previously obtained for the entire molecule using GASCOS in conjunction with AM1 and RHF/3-21G calculations. Thus, these results are an additional support for this systematic conformational search using the entire molecule.

In Figure 6 AM1, RHF/3-21G, and RHF/6-31G(d) energies are plotted versus rotation angles θ_1 (a) and θ_2 (b). The energy scales in these figures are not the same in an attempt to make differences as clear as possible. The first observation was that for all the curves (Figure 6) AM1 calculations predicted extremely low-energy barriers (compare the AM1 curves with those obtained from *ab initio* calculations). It appears that the AM1 method underestimates the energetic requirement for the different conformational interconversions. These results are in

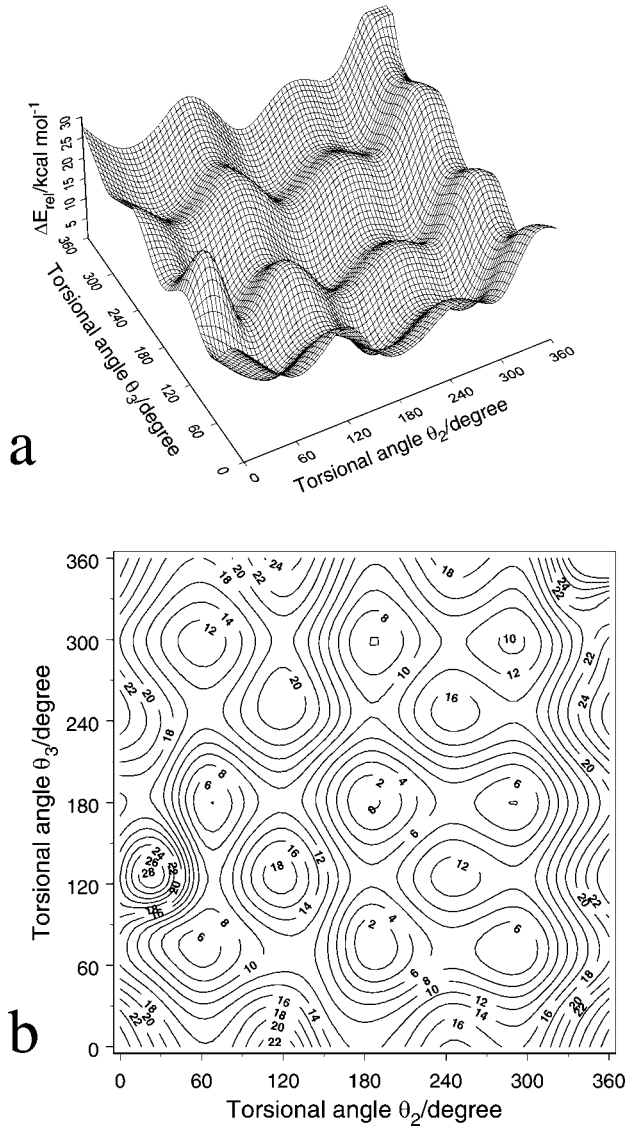

Figure 5. Potential energy surface (PES), $E = E(\theta_2, \theta_3)$, obtained for the reduced model system shown in Scheme 4B. Calculations were performed at the RHF/3-21G level. Full cycle rotation (from 0° to 360°) is shown for variables θ_2 and θ_3. (a) Energy landscape and (b) energy contour representation. The isoenergy curves are shown, each 2 kcal·mol^{-1}.

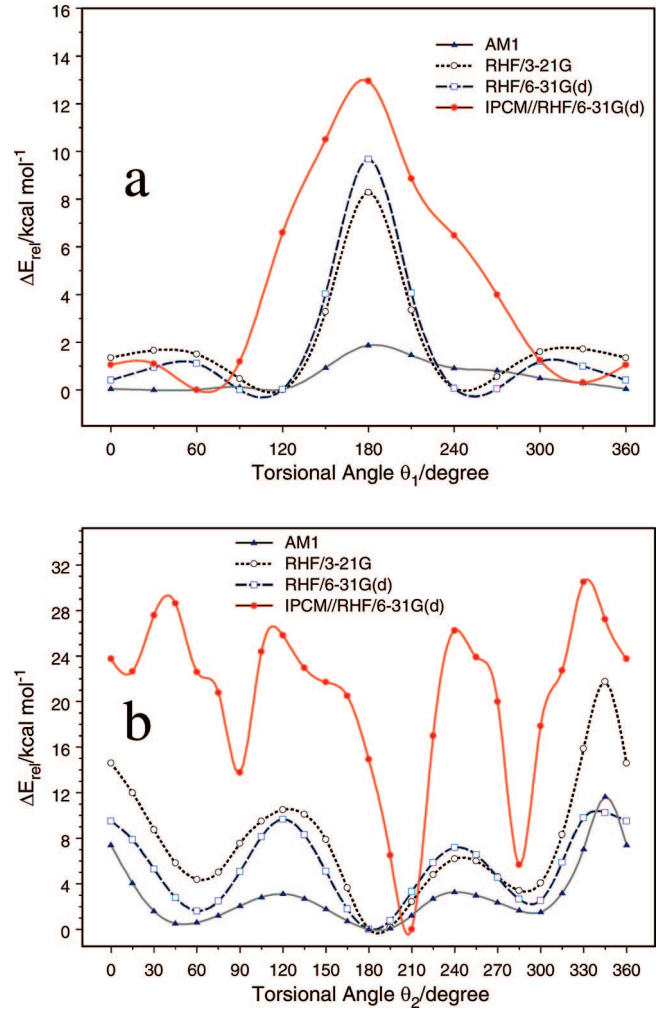

Figure 6. Comparison of PECs of torsional angles θ_1 (a) and θ_2 (b) obtained for the reduced model systems calculated at AM1, RHF/3-21G, RHF/6-31G(d), and IPCM/RHF/6-31G(d) levels of theory.

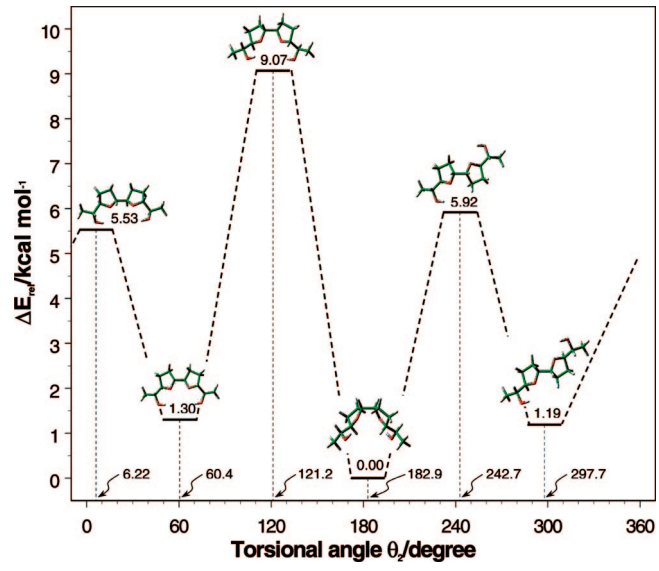

Figure 7. Critical points (minima and transition states) obtained for the reduced model system (Scheme 4B) from RHF-6-31G(d) calculations. The energy feature is also shown in this figure.

agreement with the different energy gaps between the conformers obtained using either AM1 or *ab initio* calculations. The torsion angle θ_1 (Figure 6a) displays extended shallow low-energy regions between 0° to 120° and 240° to 360°. The *ab initio* barriers at 180° were relatively high (8.28 and 9.68 kcal·mol^{-1} at RHF/3-21G and RHF/6-31G(d) levels, respectively), indicating a steric repulsion of the carbonyl group of the LR. For the torsional angle θ_2, a characteristic 3-fold symmetry PEC was obtained (Figure 6b). The global minimum was obtained for $\theta_2 \cong 180°$, and two local minima were obtained with $\theta_2 \cong 60°$ and 300°. The rotational barrier at $\theta_2 \approx 120°$ and 240° is 9.67 and 7.18 kcal·mol^{-1}, respectively, at the RHF/6-31G(d) level, indicating that the molecular flexibility of the THF rings was somewhat restricted. In order to evaluate more accurately the critical points (minima and transition states) involved in this conformational interconversion, the three minima and their respective transition structures were optimized using RHF/6-31G(d) calculations (Figure 7). These critical points indicated that the energy requirement for the conformational interconversion was somewhat lower in comparison to those obtained from the PEC (9.07 and 5.92 kcal·mol^{-1} for 120° and 240°, respectively). However, these differences might be explained considering that the PEC was calculated without

full optimization (see Figures 6 and 7). With respect to the torsional angle θ_5 (Scheme 4C), it must be pointed out that, in the literature, there are several calculations reported for closely related molecular systems,[67,68] and therefore, we did not recalculate this PEC. We have previously reported density functional theory (DFT) results for a very similar molecular system.[69] Our results indicated that this PEC displayed a relatively low rotational barrier ($\cong$3.0 kcal·mol^{-1}) nearly 120° and 240° at the B3LYP/6-31G(d) level. These results indicated that the connecting chain possessed a significant molecular flexibility at least in the gas phase.

We assume that solvent effects might somewhat change these results. To verify the assumption, this effect was added to the computations. For this purpose, the IPCM method was adopted, which defined the cavity as an isodensity surface of the molecule. For torsional angle θ_1, it was seen that the conformational allowed space for the hydrated model system was substantially reduced with respect to the isolated molecule. However, different conformations were still available (Figure 6a). Figure 6b presents the results of torsional angle θ_2 in the hydrated system, and also in this case some differences were observed in comparison with the results obtained for the isolated molecule depicted in the same figure. Instead of three minima (g^+, a, and g^-) of almost the same energy, we observed here a deep minimum for the *anti* form. Also, the energy barriers between the *gauche* and *anti* conformers were very large, indicating that a conformation with $\theta_2 \cong 200°$ was the only available form. Our previous results using IPCM/DFT calculations for a similar system to that of the θ_5 torsional angle indicated that the effect of the solvent on this portion was also significant.[69] Once again, the energy barrier for this torsion angle, considering the solvent effects, was larger than that of the isolated molecule. Observing the PECs of Figure 6 as well as the previously reported DFT results,[69] it is evident that *ab initio*/IPCM and DFT/IPCM calculations predicted energy barriers higher than those obtained using *ab initio* and DFT gas-phase computations.

In short, the above results appear to indicate that the structure of bullacin B in water is not as flexible as we expected from the gas-phase results. Thus, at this stage of our work, we consider the trend predicted for the solution effects as certainly significant. To better evaluate the conformational behavior of bullacin B considering the effects of the solvent, an MD simulation of bullacin B was performed using two different solvents. These results are presented in the following section.

3.2. MD Simulations. In a first step, we performed MD simulations of bullacin B using only water as solvent. These results were very different from those of the systematic conformational search in the gas phase. MD simulations predicted a high preference for the folded and fully folded forms. Figure 8 shows the values obtained for the $C_{20}-C_2$ distance which displays the general spatial ordering of the connecting chain during simulation. The short distances obtained ($\cong$6 Å) clearly demonstrated that bullacin B (in water) was maintained in a fully folded conformation for most of the simulation time. An extended form was chosen as the starting conformation for the simulation, although this initial conformation changed at 2.7 ns to a folded one, and then folded and fully folded forms were maintained for 50 ns of simulation. This result was not unexpected. Bullacin B (and ACG in general) possessed extensive hydrophobic portions; therefore, it was reasonable that this molecule displayed a marked tendency to adopt folded or fully folded forms in order to avoid the interaction between the hydrophobic portions with a polar solvent (water in this case).

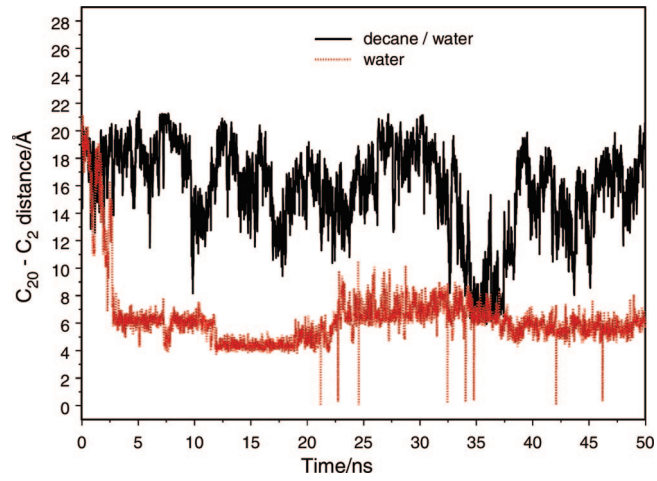

Figure 8. Time evolution of the $C_{20}-C_2$ distance during the 50 ns of simulation using water and decane/water systems. This figure shows the general spatial ordering of the connecting chain of bullacin B.

Besides, we were interested in the conformational behavior of bullacin B not only in the gas-phase and in aqueous solution but also near complex I. Therefore, a different solvent system is necessary to simulate such a situation. We need to simulate an environment considering not only the water but also the hydrophobic portion of the biological membrane. Thus, decane was chosen to mimic the membrane environment. Clearly, decane lacks a number of important features of real membranes, including polar headgroups and the associated charge distribution, the structured long lipid tails, and the nonuniform density and pressure profiles of real lipid bilayers of micelles. However, the use of a decane/water system has many advantages such as a decent representation of water and of the hydrophobic membrane interior and the computational simplicity. Also, the dynamics of decane is much faster than that of lipids, and the motions of peptides in hydrocarbons are faster than those in lipids as well. In addition, this system has been previously tested[53] and also employed with very good results in other compounds.[70,71]

Comparing the $C_{20}-C_2$ interatomic distances obtained during the MD simulations using water and decane/water (Figure 8), these results were completely different. Whereas, in water, a fully folded form was practically the only possible form for the connecting chain of bullacin B, in decane/water this chain may adopt different forms, from folded (more than 6 Å) to fully extended forms ($\cong$21 Å). However, it should be noted that during the MD simulation using decane/water the connecting chain hardly adopted the fully folded form. This was a striking difference with respect to the MD simulation using only water as solvent. Figure 9 shows the different values adopted by the virtual angle γ during the 50 ns of simulation using decane/water as solvent. It is interesting to note that bullacin B was visiting all five families (I, LO, L, LC, and V) as well as many of the different 125 subfamilies previously classified according to the spatial ordering of the connecting chain. However, comparing the percentage of population obtained from this MD simulation with those attained from the systematic search (Table 2), it is clear that there were some differences. Whereas semiempirical and *ab initio* methods favored the L and I forms, MD simulation preferred the V form. Although MD simulations performed here cannot guarantee the completeness of the conformational search, from our results it appears that MD simulations were as efficient as the systematic search to find most of the different conformation types of bullacin B. However,

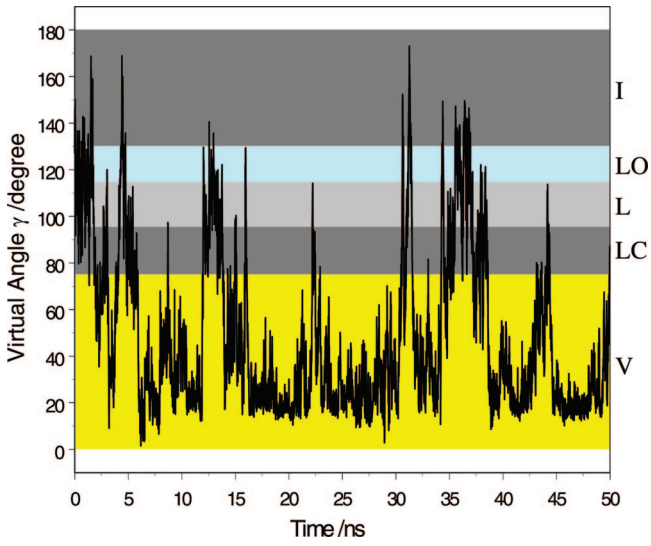

Figure 9. Variation of the virtual angle γ during the 50 ns of simulation using the decane/water system. The correlation between the values of the virtual angle γ and the five families is shown on the right.

it is clear that for MD simulations it is necessary to properly include the effects of solvents.

In order to further compare MD simulations with the *ab initio* results, the torsional angles θ_1 and θ_2 obtained from MD simulations using the decane/water system were plotted. Figure 10 shows the evolution of angles θ_1 (Figure 10a) and θ_2 (Figure 10b) as a function of time. Angle θ_1, which represented the rotation of LR, displayed a significant flexibility ($-120° \geq \theta_1 \leq 120°$). In contrast, angle θ_2, which represented the bond between both THF rings, oscillated around the mean value (180°) without great changes, indicating a restricted rotation. This result was in agreement with the results obtained from AM1 and *ab initio* calculations, in particular with that obtained from IPCM, predicting that a conformation with $\theta_2 \cong 200°$ was the only available form. In order to evaluate the conformational behavior of the torsional angles involved in the connecting chain, we plotted the evolution of one of their rotations (the torsional angle φ_{18}, Figure 1) as a function of time (Figure 10c). The 3-fold periodicity (60°, 180°, and 300°) might be appreciated in this figure. It is interesting to note that these results obtained from MD simulations for the whole molecule were in complete agreement with the PECs obtained from QM/OM calculations using a reduced model system (see Figure 6).

Both MD simulations, using water and decane/water, indicated that the hydrophobic tail displayed a clear tendency to adopt extended or fully extended forms. Figure 11 shows the values of the $C_{34}-C_{20}$ distance obtained during the simulation. It is clear from this figure that the hydrophobic tail preferred to adopt a fully extended form (≅16.5 Å) or partially extended form (≅12 Å). This result is an additional support for our previous assumption about this portion which can be fixed in an extended form as it was considered in the systematic search.

In order to get a graphical representation of the average position of bullacin B relative to the solvent, the partial density profiles were calculated as a function of the z coordinate for each of the three system components (bullacin B, decane, and water) and averaged over the simulation time (Figure 12a). The analysis of the partial density profile in each MD run showed that bullacin B was located near the interface for all the simulations (it ranged from 1.1 to 2.2 nm from the bottom of the box). More precise information about the orientation of the relevant portions of bullacin B can be obtained from the analysis

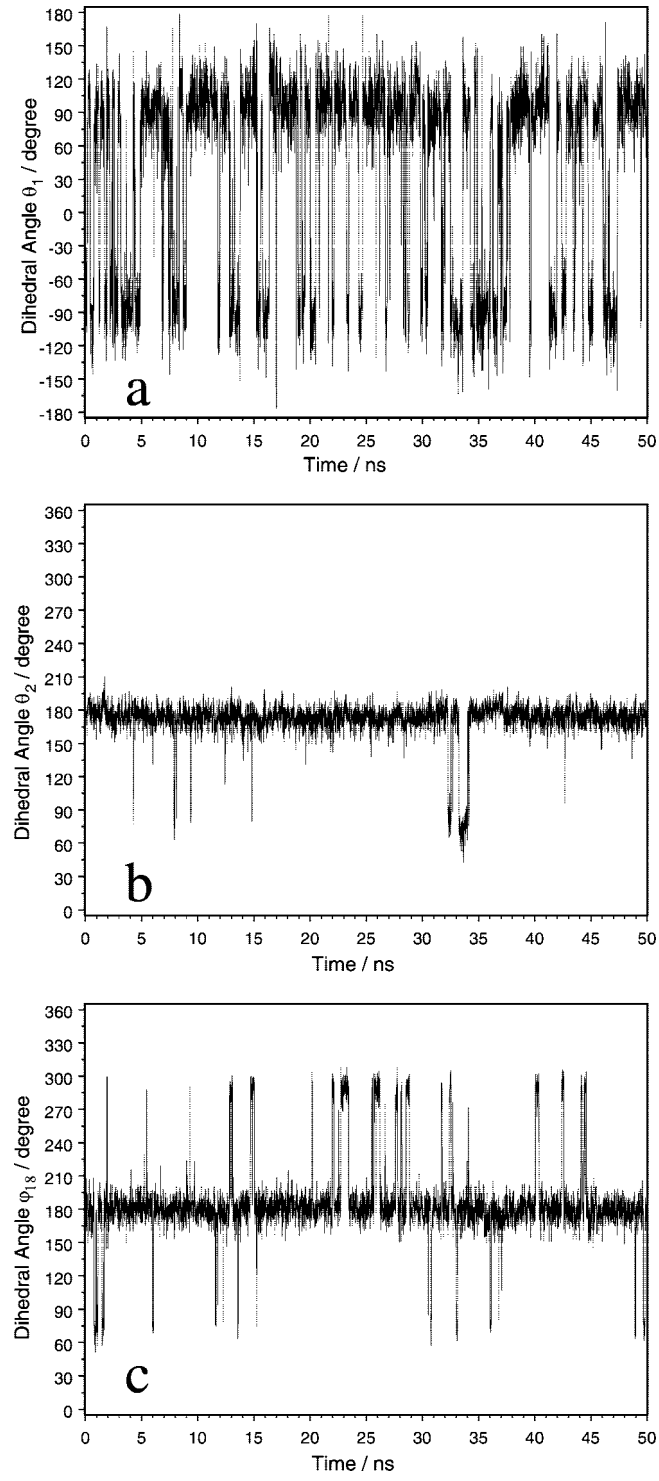

Figure 10. Temporal evolutions of dihedral angles θ_1 (a), θ_2 (b), and φ_{18} (c) during the 50 ns of simulation using the decane/water system.

of the average position of each moiety along the z axis. The density profile of the LR and THF portions was calculated and averaged over the z coordinate in the MD trajectory (Figure 12b). Approximately 90% of the partial density of the LR moiety ranged between 1.1 and 1.6 nm from the bottom of the box, while that of the THF portion ranged from 1.2 to 2.2 nm (Figure 12b). The density profile of both moieties showed only one maximum with a relatively narrow distribution, meaning that the orientation of each ring was quite stable and near the interface on the time scale of 50 ns. The spatial positions of

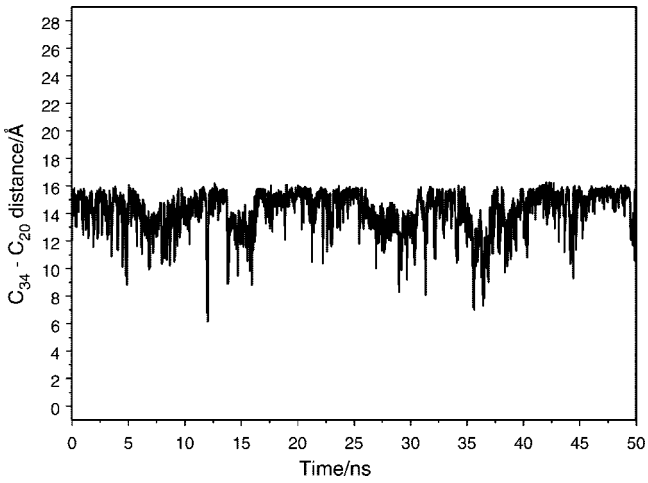

Figure 11. Time evolution of the $C_{34}-C_{20}$ distance showing the spatial ordering adopted by the hydrophobic tail during the simulation time.

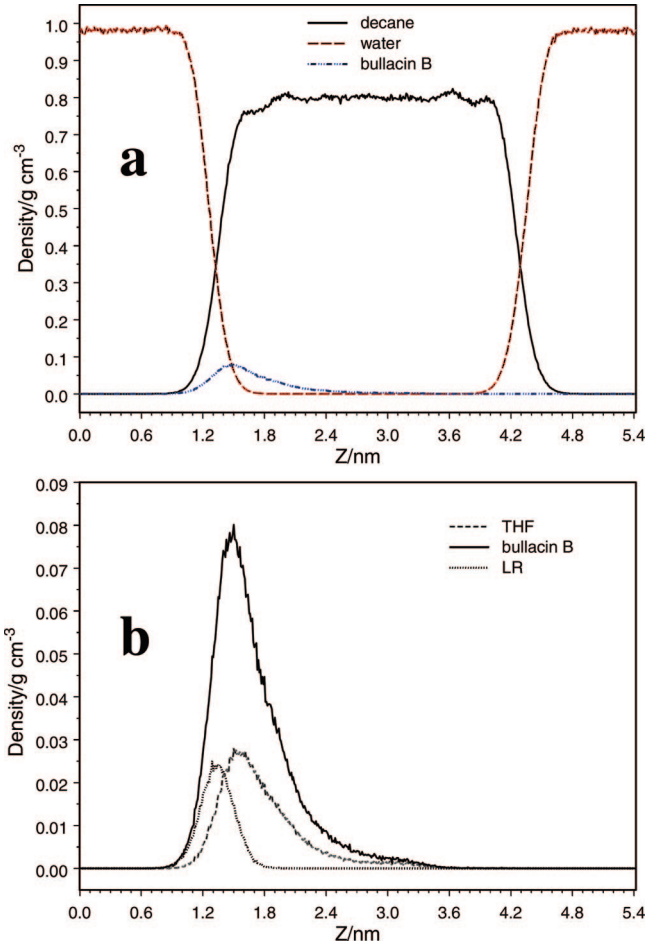

Figure 12. (a) Density profile of the bullacin B/decane/water system averaged over 50 ns in the *z* direction. (b) Density profiles of bullacin B and two selected groups (THF and LR) averaged over 50 ns of the MD run.

LR and THF might be well appreciated from Figure 13. Figure 13a shows that LR was located exactly in the interface for all the simulation times, whereas THF was slightly shifted to the hydrophobic face though still near the interface zone (Figure 13b).

We have recently reported a MD simulation of diacetylguanacone (d-GUA) in a full hydrated l-palmitoyl-2-oleoyl-*sn*-glycero-3-phosphatidylcholine (POPC)[26] bilayer. From these

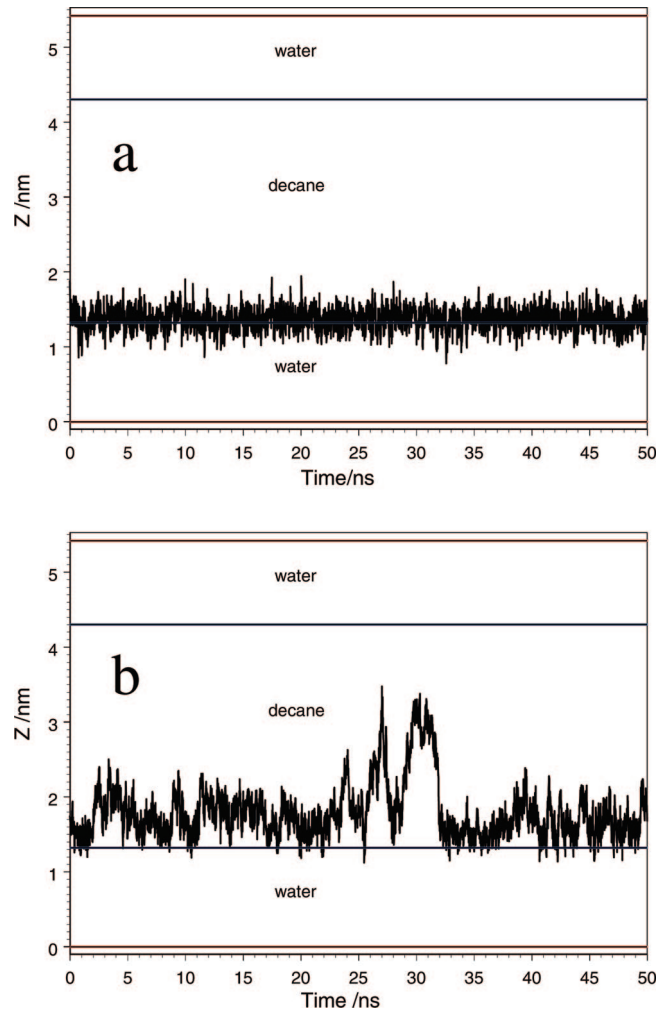

Figure 13. Different positions of LR (a) and THF (b) as function of time.

results, a putative "biologically relevant conformation" for d-GUA was proposed. The LR and THF moieties located in the interface of the lipid bilayer characterized this conformation. The proposed biologically relevant conformation was a characteristic L form; however, the MD simulation indicated that d-GUA embedded in the POPC possessed a significant molecular flexibility. Our MD results using decane/water as solvent were in complete agreement with those previously reported.[26]

Figure 14 shows a snapshot of the bullacin B/decane/water system at 13 ns of the MD simulation where bullacin B adopted an L conformation. The position of both rings, LR and THF, near the interface zone might be appreciated in this figure. It is interesting to remark that the conformational behavior obtained for bullacin B using the decane/water system as solvent was closely related to that previously reported for d-GUA embedded in the POPC bilayer.[26] Considering the significant lower computational requirements to simulate the decane/water system instead of a complex complete lipid membrane, the decane/water interface appeared to be an excellent reduced system to simulate the conformational behavior of ACGs in their biological environment.

3.3. Molecular Electrostatic Potentials (MEPs). The electronic study of bullacin B was performed using MEPs. Different low-energy conformations were used for this study, although all of them displayed the same general electronic distribution. The salient feature of this MEP was the existence of four clearly different regions, two polar regions possessing negative as well

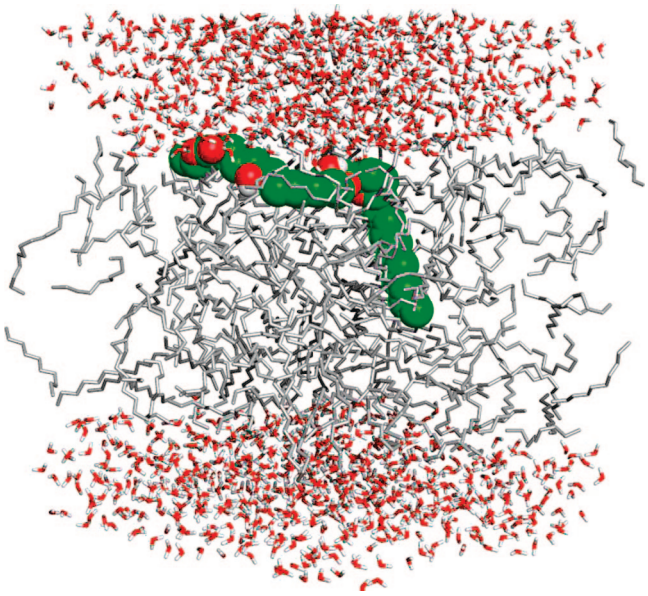

Figure 14. Snapshot of the location of bullacin B taken at 13 ns of the simulation. The conformation type "L" adopted by bullacin B might be appreciated in this figure.

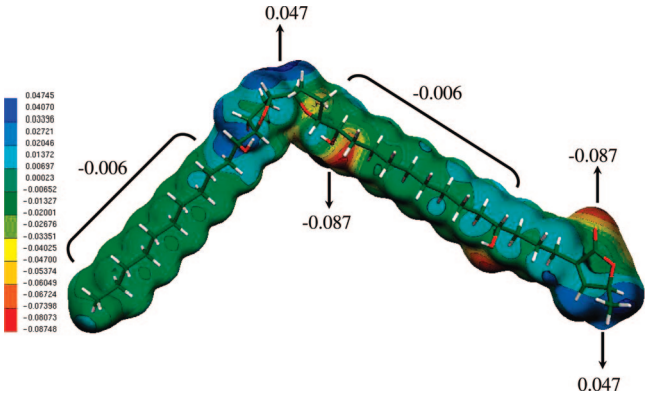

Figure 15. Electrostatic potential-encoded electron density surfaces of bullacin B. The surfaces were generated with Gaussian03 using RB3LYP/6-31G(d) single point calculations. The coloring represents electrostatic potentials with red indicating the strongest attraction to a positive point charge and blue indicating the strongest repulsion. The electrostatic potential is the energy of interaction of the positive point charge with the nuclei and electrons of a molecule. It provides a representative measure of the overall molecular charge distribution. The color code is shown on the left.

as positive potentials, and two hydrophobic zones with almost neutral values of $V_{(r)}$ (Figure 15). The hydrophobic regions corresponded to the connecting chain and to the so-called hydrophobic tail, whereas the polar regions corresponded to the lactone ring and the THF domain. These results indicated that bullacin B possessed two important hydrophobic zones which were in agreement with the results obtained from MD simulations using different solvents.

4. Conclusions

There is in the literature some SAR studies reported on acetogenins. However, in these studies, the conformational problem of these molecules has been overlooked. We report here the first comprehensive conformational study of bullacin B, a characteristic inhibitor of complex I. The systematic search generates all possible solutions, but it is highly demanding of CPU time and storage location. Some differences appear in the ordering of the local minima depending on the quantum method used. Also, the different levels of theory reported here predict different molecular flexibility for bullacin B. For example, AM1 calculations appear to underestimate the conformational interconversions. According to our results, semiempirical calculations should carefully be used only for a preliminary or exploratory conformational analysis. At least, the Hartree−Fock level of theory in conjunction with a 6-31G(d) basis set appears to be necessary to confirm critical points at the PEHS and to assign the conformational preferences of this compound. Thus, we recommend some caution when doing structural discussions based only on the energy differences. Another important factor is the role of the surrounding medium. Bullacin B (and ACGs in general) possesses polar and hydrophobic portions in its structure; therefore, interaction forces in aqueous or biological environments introduce profound changes in the conformational behavior of this compound. It is clear that this influence has to be properly taken into account in the calculations. Explicit inclusion of solvent molecules or appropriate approximations to simulate their effects is necessary to get a better insight about the relative energies of the active conformers in living media.

Different conformations were found for bullacin B depending on the calculations method used. When applying semiempirical and *ab initio* methods, the L and I forms were favored, whereas when using MD simulation the V form was preferred. Considering the significant molecular flexibility obtained for bullacin B, it is difficult to determine which conformations might be biologically relevant for this molecule. However, on the basis of our theoretical results, it appears that the preferred L and V forms and a rapid interconversion between them might be necessary to produce the biological response. The conformational selection of the flexible acetogenins binding to a receptor can have different procedures. The mechanism of the binding process can presume two general cases: (1) At any instant, only those acetogenins having the appropriate single conformation are able to bind to the receptor. Each portion of bullacin B binds simultaneously to the appropriate subsite of the binding site. This model is associated with the idea that the preferred conformation in solution is relevant for binding. However, in this case, there is no *a priori* reason why this should be so. Also, there are a number of instances in which the conformation of a ligand bound to a protein has shown to be different from the preferred conformation in solution. (2) Another possibility is that the binding takes place by a stepwise process in which the THF rings (in any conformation) act as the anchoring portion in the interface of the lipid bilayer, and this process is followed by a rapid rearrangement of the conformation of bullacin B so as to permit the interaction of the remaining functional moiety (the lactone ring). This hypothesis assuming that the THF rings are the anchoring portion of the molecule is also in agreement with the NMR results previously reported by McLaughlin et al.[24,25] An important difference between these models is that, in the second case, the actual conformational distribution of bullacin B is less crucial, while the rate at which conformational interconversions can occur becomes considerably significant.

Accepting the validity of the *ab initio* method/MD simulations and of the obtained results, it seems that model 2 or an intermediate model sharing aspects of both models (1 and 2) is probable for bullacin B. There is not a single and particular form but a range of conformations (from partially folded to partially extended) for the alkyl spacer linking the LR and THF rings, which seems to be well tolerated to produce the biological response. However, it is clear that not any conformation may be operative. A high-energy barrier might force the molecule

to bind by the "all-or-none" mechanism (model 1) rather than by the zipper mechanism (model 2). RHF/6-31G(d) calculations predict that barriers about $\cong 3-9$ kcal·mol^{-1} are separating the different conformations, and therefore, the conformational interconvertions are somewhat restricted but still available for bullacin B. Also, a large part of the conformationally available space is accessible within a low value of energy with respect to the global minimum. Note that MD simulations predict that bullacin B is visiting all the five families (I, LO, L, LC, and V) as well as many of the different 125 subfamilies previously classified according to the spatial ordering of the connecting chain. This is an additional support for model 2 or an intermediate model.

The theoretical results reported here were tested and compared to evaluate bullacin B for future conformational analysis involving relatively large-size flexible molecules (such as ACGs) for which a complete grid search is expensive in terms of calculation time. In this sense, our results support the use of the MD simulations for bullacin B, although the aqueous and biological environment influence has to be properly taken into account in these simulations. It appears that a combined decane/water system is good enough to simulate the biological environment of this molecule. Such simulations can provide important information about the preferred conformations and molecular flexibility of ACGs, which might be useful when deciding which conformations to include in a docking algorithm. In addition, MD simulations using the decane/water system as a membranelike phase might allow us to evaluate a great number of different acetogenins to perform SAR and/or QSAR studies considering the conformational problem but using a reasonable computer time.

Acknowledgment. This work was supported by grants from Universidad Nacional de San Luis. R.D.E. is member of the Consejo Nacional de Investigación Científica y Tecnológica (CONICET, Argentina) staff. M.F.M is a fellow of CONICET.

Supporting Information Available: Table S1, conformations obtained from AM1 optimizations; Table S2, conformations optimized using RHF/3-21G calculations. This material is available free of charge via the Internet at http://pubs.acs.org.

References and Notes

(1) Zeng, L.; Ye, Q.; Oberlies, N. H.; Shi, G.; Gu, Z.-M.; He, K.; McLaughlin, J. L. *Nat. Prod. Rep.* **1996**, *13*, 275.

(2) McLaughlin, J. L.; Zeng, L.; Oberlies, N. H.; Alfonso, D.; Johnson, H. A.; Cummings, B. A. *Phytochemicals for Pest Control*; American Chemical Society: Washington, DC, 1997.

(3) Alali, F. Q.; Liu, X. X.; McLaughlin, J. L. *J. Nat. Prod.* **1999**, *62*, 504.

(4) Oberlies, N. H.; Chang, C. J.; McLaughlin, J. L. *J. Med. Chem.* **1997**, *40*, 2102.

(5) Konno, H.; Hiura, N.; Makabe, H.; Abe, M.; Miyoshi, H. *Bioorg. Med. Chem. Lett.* **2004**, *14*, 629.

(6) Hollingworth, R. M.; Ahammadsahib, K. I.; Gadelhak, G.; McLaughlin, J. L. *Biochem. Soc. Trans.* **1994**, *22*, 230.

(7) Degli Esposti, M.; Ghelli, A.; Ratta, M.; Cortes, D.; Estornell, E. *Biochem. J.* **1994**, *301*, 161.

(8) Okun, J. G.; Lümmon, P.; Brandt, U. *J. Biol. Chem.* **1999**, *274*, 2625.

(9) Friedrich, T.; Van Heek, P.; Leif, H.; Ohmishi, T.; Forche, E.; Kunsen, B.; Jansen, R.; Trowitzsch-Kienast, W.; Höfle, G.; Reichenbach, H.; Weiss, H. *Eur. J. Biochem.* **1994**, *219*, 691.

(10) Miyoshi, H. *J. Bioenerg. Biomembr.* **2001**, *33*, 223.

(11) Duval, R. A.; Lewin, G.; Peris, E.; Chahboune, N.; Garofano, A.; Dröse, S.; Cortes, D.; Brandt, U.; Hocquemiller, R. *Biochemistry* **2006**, *45*, 2721.

(12) Chahboune, N.; Barrachina, I.; Royo, I.; Romero, V.; Sáez, J.; Tormo, J. R.; De Pedro, N.; Estornell, E.; Zafra-Polo, M. C.; Peláez, F.; Cortes, D. *Bioorg. Med. Chem.* **2006**, *14*, 1089.

(13) Abe, M.; Murai, M.; Ichimaru, N.; Kenmochi, A.; Yoshida, T.; Kubo, A.; Kimura, Y.; Moroda, A.; Makabe, H.; Nishioka, T.; Miyoshi, H. *Biochemestry* **2005**, *44*, 14898.

(14) Takada, M.; Kuwabara, K.; Nakato, H.; Tanaka, A.; Iwamura, H.; Miyoshi, H. *Biochim. Biophys. Acta* **2000**, *1460*, 302.

(15) Hoppen, S.; Emde, U.; Friedrich, T.; Grubert, L.; Koert, U. *Angew. Chem., Int. Ed.* **2000**, *39*, 2099.

(16) Tormo, J. R.; Estornell, E.; Gallardo, T.; González, M. C.; Cavé, A.; Granell, S.; Cortes, D.; Zafra-Polo, M. C. *Bioorg. Med. Chem. Lett.* **2001**, *11*, 681.

(17) Tormo, J. R.; Gallardo, T.; Peris, E.; Bermejo, A.; Cabedo, N.; Estornell, E.; Zafra-Polo, M. C.; Cortes, D. *Bioorg. Med. Chem. Lett.* **2003**, *13*, 4101.

(18) Yabunaka, H.; Abe, M.; Kenmochi, A.; Hamada, T.; Nishioka, T.; Miyoshi, H. *Bioorg. Med. Chem. Lett.* **2003**, *13*, 2385.

(19) Makabe, H.; Miyawaki, A.; Takahashi, R.; Hattori, Y.; Konno, H.; Abe, M.; Miyoshi, H. *Tetrahedron Lett.* **2004**, *45*, 973.

(20) Abe, M.; Kenmochi, A.; Ichimaru, N.; Hamada, T.; Nishioka, T.; Miyoshi, H. *Bioorg. Med. Chem. Lett.* **2004**, *14*, 779.

(21) Motoyama, T.; Yabunaka, H.; Miyoshi, H. *Bioorg. Med. Chem. Lett.* **2002**, *12*, 2089.

(22) Kuwabara, K.; Takada, M.; Iwata, J.; Tatsumoto, K.; Sakamoto, K.; Iwamura, H.; Miyoshi, H. *Eur. J. Biochem.* **2000**, *267*, 2538.

(23) Hamada, T.; Ichimaru, N.; Abe, M.; Fujita, D.; Kenmochi, A.; Nishioka, T.; Zwicker, K.; Brandt, U.; Miyoshi, H. *Biochemistry* **2004**, *43*, 3651.

(24) Shimada, H.; Grutzner, J. B.; Kozlowski, J. F.; McLaughlin, J. L. *Biochemistry* **1998**, *37*, 854.

(25) Shimada, H.; Kozlowski, J. F.; McLaughlin, J. L. *Pharmacol. Res.* **1998**, *37*, 357.

(26) Barrachina, I.; Royo, I.; Baldoni, H.; Chahboune, N.; Suvire, F.; DePedro, N.; Zafra-Polo, M. C.; Bermejo, A.; Cabedo, N.; Saez, J.; Tormo, J. R.; Enriz, R. D.; Cortes, D. *Bioorg. Med. Chem.* **2007**, *15*, 4369.

(27) Peterson, M. R.; Csizmadia, I. G. *J. Am. Chem. Soc.* **1978**, *100*, 6911.

(28) Peterson, M. R.; Csizmadia, I. G. *Prog. Theor. Org. Chem.* **1982**, *3*, 190.

(29) Miyoshi, H.; Ohshima, M.; Shimada, H.; Akagi, T.; Iwamura, H.; McLaughlin, J. L. *Biochim. Biophys. Acta* **1998**, *1365*, 443.

(30) Hopp, D. C.; Alali, F. Q.; Gu, Z.; McLaughlin, J. L. *Bioorg. Med. Chem.* **1998**, *6*, 569.

(31) (a) Santágata, L. N.; Suvire, F. D.; Enriz, R. D.; Torday, L. L.; Csizmadia, I. G. *J. Mol. Struct. (THEOCHEM)* **1999**, *465*, 33. (b) Santágata, L. N.; Suvire, F. D.; Enriz, R. D. *J. Mol. Struct. (THEOCHEM)* **2000**, *507*, 89. (c) Santágata, L. N.; Suvire, F. D.; Enriz, R. D. *J. Mol. Struct. (THEOCHEM)* **2001**, *536*, 173. (d) Santágata, L. N.; Suvire, F. D.; Enriz, R. D. *J. Mol. Struct. (THEOCHEM)* **2001**, *571*, 91.

(32) Suvire, F. D.; Santagata, L. N.; Bombasaro, J. A.; Enriz, R. D. *J. Comput. Chem.* **2006**, *27*, 188.

(33) Suvire, F. D.; Sortino, M.; Kouznetsov, V. V.; Vargas, M. L. Y.; Zacchino, S. A.; Mora Cruz, U.; Enriz, R. D. *Bioorg. Med. Chem.* **2006**, *14*, 1851.

(34) Dewar, J. M. S.; Zoebisch, E. G.; Healy, E. F.; Stewart, J. J. P. *J. Am. Chem. Soc.* **1985**, *107*, 3902.

(35) Foresman, J. B.; Keith, T. A.; Wiberg, K. B.; Snoonian, J. *J. Phys. Chem.* **1996**, *100*, 16098.

(36) Miertus, S.; Scrocco, E.; Tomasi, J. *Chem. Phys.* **1981**, *55*, 117.

(37) Radkiewicz, J. L.; Clarke, S.; Zipse, H.; Houk, K. N. *J. Am. Chem. Soc.* **1996**, *118*, 9148.

(38) Jhon, J. S.; Kang, Y. K. *J. Phys. Chem. A* **1999**, *103*, 5436.

(39) Shukla, M. K.; Mishra, S. K.; Kumar, A.; Mishra, P. C. *J. Comput. Chem.* **2000**, *21*, 826.

(40) Bandyopadhyayay, P.; Gordon, M. S. *J. Chem. Phys.* **2000**, *113*, 1104.

(41) Rodríguez, A. M.; Koo, J. C. P.; Rojas, D.; Peruchena, N.; Enriz, R. D. *Int. J. Quantum Chem.* **2006**, *106*, 1580.

(42) Masman, M. F.; Lovas, S.; Murphy, R. M.; Enriz, R. D.; Rodríguez, A. M. *J. Phys. Chem. A* **2007**, *111*, 10682.

(43) Frisch, M. J.; Trucks, G. W.; Schlegel, H. B.; Scuseria, G. E.; Robb, M. A.; Cheeseman, J. R., Montgomery, J. A., Jr.; Vreven, T.; Kudin, K. N. , Burant, J. C.; Millam, J. M.; Iyengar, S. S.; Tomasi, J.; Barone, V.; Mennucci, B.; Cossi, M.; Scalmani, G.; Rega, N.; Petersson, G. A.; Nakatsuji, H.; Hada, M.; Ehara, M.; Toyota, K.; Fukuda, R.; Hasegawa, J.; Ishida, M.; Nakajima, T.; Honda, Y.; Kitao, O.; Nakai, H.; Klene, M.; Li, X.; Knox, J. E.; Hratchian, H. P.; Cross, J. B.; Bakken, V.; Adamo, C.; Jaramillo, J.; Gomperts, R.; Stratmann, R. E.; Yazyev, O.; Austin, A. J.; Cammi, R.; Pomelli, C.; Ochterski, J. W.; Ayala, P. Y.; Morokuma, K.; Voth, G. A.; Salvador, P.; Dannenberg, J. J.; Zakrzewski, V. G.; Dapprich, S.; Daniels, A. D.; Strain, M. C.; Farkas, O.; Malick, D. K.; Rabuck, A. D.; Raghavachari, K.; Foresman, J. B.; Ortiz, J. V.; Cui, Q.; Baboul, A. G.; Clifford, S.; Cioslowski, J.; Stefanov, B. B.; Liu, G.; Liashenko, A.; Piskorz, P.; Komaromi, I.; Martin, R. L.; Fox, D. J.; Keith, T.; Al-Laham, M. A.; Peng, C. Y.; Nanayakkara, A.; Challacombe, M.; Gill, P. M. W.; Johnson,

B.; Chen, W.; Wong, M. W.; Gonzalez, C.; Pople, J. A. *Gaussian 03*, revision B.01; Gaussian, Inc.: Wallingford, CT, 2004.

(44) Politzer, P.; Truhlar, D. G. *Chemical Applications of Atomic and Molecular Electrostatic Potentials*; Plenum Publishing: New York, 1991.

(45) Carrupt, P. A.; El Tayar, N.; Karlé, A.; Festa, B. *Methods Enzymol.* **1991**, *203*, 638.

(46) Greeling, P.; Langenaeker, W.; De Proft, F.; Baeten, A. *Molecular Electrostatic Potentials: Concepts and Applications. Theoretical and Computational Chemistry*; Elsevier Science B. V.: Amsterdam, 1996.

(47) Flükiger, P.; Lüthi, H. P.; Portmann, S.; Weber, J. *MOLEKEL 4.0*; Swiss Center for Scientific Computing: Manno, Switzerland, 2000.

(48) Howard, A. E.; Kollman, P. A. *J. Med. Chem.* **1988**, *31*, 1669.

(49) Cohen, N. C.; Blaney, J. M.; Humblet, C.; Gund, P.; Barry, D. C. *J. Med. Chem.* **1990**, *33*, 883.

(50) McCammon, J. A.; Karplus, M. *Acc. Chem. Res.* **1983**, *16*, 187.

(51) Berendsen, H. J. C.; van der Spoel, D.; van Drunen, R. *Comput. Phys. Commun.* **1995**, *91*, 43.

(52) Lindahl, E.; Hess, B.; van der Spoel, D. *J. Mol. Model.* **2001**, *7*, 306.

(53) van Buuren, A. R.; Marrink, S. J.; Berendsen, H. J. C. *J. Phys. Chem.* **1993**, *97*, 9206.

(54) Mark, A. E.; van Helden, S. P.; Smith, P. E.; Janssen, L. H. M.; van Gunsteren, W. F. *J. Am. Chem. Soc.* **1994**, *116*, 6293.

(55) Jorgensen, W. L.; Chandrasekhar, J.; Madura, J. D.; Impey, R. W.; Klein, M. L. *J. Chem. Phys.* **1983**, *79*, 926.

(56) van Buuren, A. R.; Berendsen, H. J. C. *Biopolymers* **1993**, *33*, 1159.

(57) Liu, H.; Muller-Plathe, F.; van Gunsteren, W. F. *J. Am. Chem. Soc.* **1995**, *117*, 4363.

(58) Miyamoto, S.; Kollman, P. A. *J. Comput. Chem.* **1992**, *13*, 952.

(59) Berendsen, H. J. C.; Postma, J. P.; van Gunsteren, W. F.; Hermans, J. *Interaction Models for water in relation to protein hydration*; D. Reidel Publishing Co: Dordrecht, 1981.

(60) Darden, T.; York, D.; Pedersen, L. *J. Chem. Phys.* **1993**, *98*, 10089.

(61) Essmann, U.; Perera, L.; Berkowitz, M. L.; Darden, T.; Lee, H.; Pedersen, L. G. *J. Chem. Phys.* **1995**, *103*, 8577.

(62) Luty, B.; Tironi, I. G.; van Gunsteren, W. F. *J. Chem. Phys.* **1995**, *103*, 3014.

(63) Zimmerman, K. *J. Comput. Chem.* **1991**, *12*, 310.

(64) Ferguson, D. M. *J. Comput. Chem.* **1995**, *16*, 501.

(65) Berendsen, H. J. C.; Postma, J. P. M.; van Gunsteren, W. F.; DiNola, A.; Haak, J. R. *J. Chem. Phys.* **1984**, *81*, 3684.

(66) Hess, B.; Bekker, H.; Berendsen, H. J. C.; Fraaije, J. G. E. M. *J. Comput. Chem.* **1997**, *18*, 1463.

(67) Hafezi, M. J.; Sharif, F. *J. Mol. Struct. (THEOCHEM)* **2007**, *814*, 43.

(68) Klauda, J. B.; Brooks, B. R., Jr.; Venable, R. M.; Pastor, R. W. *J. Phys. Chem. B* **2005**, *109*, 5300.

(69) Zamora, M. A.; Masman, M. M.; Bombasaro, J. A.; Freile, M. L.; Filho, V. C.; Lopez, S. N.; Zacchino, S. A.; Enriz, R. D. *Int. J. Quantum Chem.* **2003**, *93*, 32.

(70) Jang, S. S.; Lin, S.-T.; Maiti, P. K.; Blanco, M.; Goddard, W. A., III. *J. Phys. Chem. B* **2004**, *108*, 12130.

(71) Monticelli, L.; Pedini, D.; Schievano, E.; Mammi, S.; Peggion, E. *Biophys. Chem.* **2002**, *101*−*102*, 577.

JP801962X